Published in final edited form as:
Photochem Photobiol. 2014 March ; 90(2): 419–430. doi:10.1111/php.12179.

Photophysics of Glycosylated Derivatives of a Chlorin, Isobacteriochlorin, and Bacteriochlorin for Photodynamic Theragnostics: Discovery of a Two-Photon-Absorbing Photosensitizer†

Amit Aggarwal[1,2], **Sebastian Thompson**[1], **Sunaina Singh**[1,3], **Brandon Newton**[4], **Akeem Moore**[5], **Ruomie Gao**[4,6], **Xinbin Gu**[5], **Sushmita Mukherjee**[7], and **Charles Michael Drain**[1,8,*]

[1]Department of Chemistry, Hunter College of the City University of New York, New York, NY

[2]Department of Science, Borough of Manhattan Community College of the City University of New York, New York, NY

[3]Department of Natural Sciences, LaGuardia Community College of the City University of New York, New York, NY

[4]Department of Chemistry and Physics, State University of New York at Old Westbury, Old Westbury, NY

[5]Howard University, Washington DC

[6]Department of Chemistry and Biochemistry at Jackson State University, Jackson, MS

[7]Department of Biochemistry, Weill Cornell Medical College, New York, NY

[8]The Rockefeller University, New York, NY

Abstract

The photophysical properties of a chlorin, isobacteriochlorin, and bacteriochlorin built on a core tetrapentafluorophenylporphyrin ($TPPF_{20}$) and the non-hydrolysable para thioglycosylated conjugates of these chromophores are presented. The photophysical characterization of these compounds was done in three different solvents to correlate to different environments in cells and tissues. Compared to $TPPF_{20}$ these conjugates have greater absorption in the red region of the visible spectrum and greater fluorescence quantum yields. The excited state lifetimes are from 3-11 nsec. The radiative and non-radiative rate constants for deactivation of the excited state were estimated from the fluorescence quantum yield and excited state lifetime. The data indicates that the bacteriochlorin has strong absorption bands near 730 nm and efficiently enters the triplet manifold. The isobacteriochlorin has a 40-70% fluorescence quantum yield depending on solvent, so it may be a good fluorescent tag. The isobacteriochlorins also display enhanced 2-photon absorption, thereby allowing the use of 860 nm light to excite the compound. While the 2-photon cross section of 25 GM units is not large, low light and low chromophore concentrations can induce apoptosis. The glycosylated compounds accumulate in cells and a head and neck squamous carcinoma xenograft tumor model in mice. These compounds are robust to photobleaching.

†This paper is part of the Special Issue honoring the memory of Nicholas J. Turro

*Corresponding author: cdrain@hunter.cuny.edu (C.M. Drain).

Supplementary Materials: UV-visible and fluorescence spectra in the different solvents, 2-photon data, and details of the bioimaging methods can be found at DOI: 10.1562/2006-xxxxxx.s1.

Introduction

Porphyrinoids have been studied extensively for a variety of applications such as dyes for solar energy harvesting, catalysts, and sensors for biological processes such as glucose transportation (1). These macrocycles are also extensively studied as photodynamic therapeutic (PDT) agents for the treatment of a variety of diseases such as cancer and infections (2-5). There is significant research aimed to improve both the photophysical and bio-targeting properties of PDT agents (6, 7). For both diagnostic and PDT applications, the use of the lower energy light is an important photophysical property for next generation chromophores because red to near infrared (IR) light penetrates deeper into tissues (7-9). Reduced porphyrins have stronger and redder lowest energy absorption bands (10-12). Glycosylation targets many cancer types because of the significantly increased glucose transporters and lectin-type receptors in the membrane (13-15). Carbohydrate–protein interactions are essential to a large number of biological processes such as metastasis (16), receptor-mediated endocytosis, inflammation, and infections by pathogens (13). As noted by Warburg, cancer cells consume glucose and produce lactic acid under aerobic conditions (17, 18). There are many recent reports of glyco-photosensitizers (19). Non-hydrolysable sugars appended to PDT agents such as porphyrinoids minimizes cleavage of the targeting motifs by enzymes and low pH around cancer tissues, in lysosomes, and in endosomes (20-24).

Chlorins are porphyrinoids with one pyrrole double bond missing, while isobacteriochlorins, and bacteriochlorins have two double bonds missing on the adjacent and opposite pyrroles, respectively. Oxidative and reductive transformations are used to form the natural and synthetic chromophores (10, 25, 26). Porphyrins, chlorins, isobacteriochlorins, and bacteriochlorins each have unique photophysical properties that are exploited by nature (27) and can be used for diverse applications (1). The Gouterman four-orbital model generally explains the consequences of reducing the double bonds on the frontier molecular orbitals (28-31). For example, the intensity of the lowest energy UV-visible absorption band (Q_y) in the red region progressively increases and red shifts as the number of missing double bonds increases: porphyrins to chlorins to isobacteriochlorins to bacteriochlorins. The typical fluorescence quantum yield (Φ_f) for porphyrins, chlorins and bacteriochlorins is 0.10, 0.25, and 0.15, respectively (32). Metalation of the macrocycle further modulates the photophysical properties, e.g. the enhanced spin-orbit coupling of Pd(II) and Pt(II) complexes nearly quantitatively shunts the excited state into the triplet manifold (33-35) while Ni(II) complexes form non-luminescent metal centered d,d states (36, 37). Thus, chlorins are widely studied as second generation PDT agents (38, 39), and recently bacteriochlorins are reported for this application (23, 40-42). Conjugated exocyclic chalcones are another means to extend the low energy absorption into the red (43).

To understand the potential therapeutic or diagnostic value of chromophores, the photophysical properties such as the fluorescence quantum yield, singlet state lifetime, triplet quantum yield, and the quantum yield of singlet oxygen formation are evaluated (44). For therapies, red light absorption, efficient intersystem crossing to the triplet manifold, and suitable triplet lifetimes are needed to maximize the photosensitized formation of singlet oxygen. Singlet oxygen is the initiation point for the formation of reactive oxygen species that elicit cell stress and/or death from oxidative damage at multiple sites, including mitochondria, endoplasmic reticulum, cell membranes (7). For luminescent diagnostics and trackers for biochemical applications, the fluorescence quantum yield should be optimized. A chromophore with a balance between the singlet and triplet quantum yields can potentially be used for both detection and treatment (theragnostic), but must have efficient and robust targeting motifs.

Two photon absorption (2PA) is the simultaneous absorption of two low energy photons to produce the same excited state of the dye as when excited with a single photon of twice the energy (45). 2PA fluorescence microscopy technologies are being developed for biochemical studies, pathology, and imaging applications (46, 47). Chromophores with significant 2PA cross sections are another avenue towards using red light to photosensitize the formation of singlet oxygen (48). Because red light penetrates deeper into tissues, endogenous biomolecules have a small 2PA cross section, and the high light flux needed to simultaneously absorb two photons, the phototoxicity is confined to the narrow area where the light flux is greatest ($\sim$0.1 mm^2) (49, 50).

Most porphyrin derivatives have small 2PA cross sections (45, 51). Peripherally appended 2PA dyes can transfer energy to a porphyrin core (52-54). Ethyne or butadiyne-bridged porphyrin dimers and oligomers (55-57), self-assembled ethyne or butadiyne-bridged arrays (58, 59), and aggregates (60, 61) are reported to have large 2PA cross sections. Some water soluble and glycosylated yne-linked 2PA systems are also reported (48, 62-64). Some of these systems may also have significant single photon absorptions in the same near IR region (65). The large molecular size of these systems may be a limiting factor in their practical applications as PDT agents.

We reported that 5,10,15,-20-tetrakis(2,3,4,5,6-pentafluorophenyl)porphyrin ($TPPF_{20}$) can serve as a core platform to make non-hydrolysable glycosylated porphyrins (20-22) and solution phase combinatorial libraries appended with a variety of bio-targeting motifs (66, 67). The non-hydrolysable tetraglucose derivative ($PGlc_4$) is a quite selective and effective PDT agent in vitro studies using several cancer cell lines, such as MDA-MB-231 human breast cancer cells (21, 22). Low light irradiation and <1 μM porphyrin concentrations induce apoptosis predominantly by damage to the endoplasmic reticulum (68). $TPPF_{20}$ is readily modified to form the corresponding chlorin ($ChlF_{20}$), isobacteriochlorin ($IbacF_{20}$), and bacteriochlorin ($BacF_{20}$) (69). We recently reported that these can be thioglycosylated in high yield to form $CGlc_4$, $IGlc_4$, and $BGlc_4$ (Scheme 1) using the same click-type chemistry and that these are also taken up by cancer cells (23, 24).

Herein we describe the photophysical properties of this series of porphyrinoids. The overall goal is to study the photophysical properties of these new compounds to assess their potential in applications such as biomarkers and therapeutics under normal, single photon, and two photon excitation conditions. The results presented here suggest that a single porphyrin dye molecule, as opposed to a multichromophoric system, can possess a sufficient two-photon cross section to be a good two photon imaging agent. Specifically, $IbacF_{20}$, and $IGlc_4$ have a sufficient 2PA and emission to obtain high quality two photon microscopy images. These results also suggest that $IGlc_4$ is a good candidate for simultaneous imaging and PDT using near IR light. Because of significantly stronger Q bands at 730 nm and high triplet quantum yield, $BGlc_4$ has good potential as a PDT agent under single photon conditions. The $CGlc_4$ has intermediate photophysical properties that may be used for both detection and ablation of cancer.

Materials and Methods

$TPPF_{20}$ was purchased from Huhu Technology or Frontier Scientific and used as received; solvents from Fisher Scientific were purified by standard methods and reagents from Sigma-Aldrich.

UV-visible spectroscopy

The UV-visible spectra were recorded on a Varian Bio3 spectrophotometer using 1 cm cuvettes. The UV-visible data for the glycosylated conjugates were reported earlier (23) and

are in the Supplementary Materials for clarity. The concentrations of each solution were ca. 1 μM.

Fluorescence spectra and quantum yield

Fluorescence spectra and time correlated single photon counting (TCSPC) were recorded with a Fluorolog τ3, Jobin-SPEX Instrument S.A., Inc. (23) on ∼1 μM solutions in ethanol and ethylacetate. Samples were excited at the same band (∼509 nm) where absorbencies ≤ 0.1 and were within 10% of each other. For emission spectra, both the excitation and detection monochromators had a band pass of 2 nm. The corrected emission (for instrument response) and absorption spectra were used to calculate the quantum yield. Fluorescence quantum yields were determined for these non-glycosylated F_{20} analogues in solution relative to *meso*-tetraphenylporphyrin (TPP) in toluene, which has a fluorescence quantum yield of 0.11 (70, 71).

Fluorescence lifetime

TCSPC fluorescence lifetime of non-glycosylated F_{20} and glycosylated conjugates were determined in three different solvents: ethanol, ethylacetate, and phosphate buffered saline (PBS). A 405 nm NanoLED laser, average power 13.6 pJ/pulse with a source pulse width <200 ps was used to excite the molecules. The instrument has 200 ps resolution. The data was fit using the instrument software.

Photobleaching

Photo stability was assayed by exposing 1μM solutions of these conjugates in ethanol to sun light with a power of 40-80 W/m^2 for about 2 hours and taking the UV-visible spectra (see Supplementary Materials).

Octanol/water partition coefficient

The octanol/water partition coefficients were determined by saturating 1:1 (v/v) mixtures of the solvents with the thioglycosylated porphyrinoids. We shook the mixture well and waited for 8-10 h to assure the two layers were separated completely. UV-visible spectra of the two layers were then taken to measure the Soret (B) and first Q-band intensities of the thioglycosylated compounds. This data were confirmed by saturating each solvent separately before mixing equal volumes (23).

Confocal microscopy

To check the photo stability of $CGlc_4$ in cells, confocal microscopic measurements were done. K:Molv NIH 3T3 cells were plated onto cover slips in cell culture dishes. $CGlc_4$ dissolved in methanol was added to the cultures to a final concentration of 0.1 μM. After incubation for 24 h, the cells were rinsed three times with PBS and incubated with a 4% paraformaldehyde solution for 15 min at 37 °C under cell growth conditions. Cells were then washed three times with PBS, mounted in Dako fluorescence mounting medium, and visualized using a Zeiss LSM510 laser scanning confocal microscope. The cells were exposed to the laser light and images were captured. An oil immersion objective lens (Leica, Fluor-40X, NA 1.25) was used for cell imaging. Images were captured with excitation at 552 nm and the emission band pass filter was 578-700 nm. The two photon microscope was used to investigate the photo stability of $IbacF_{20}$ on the same cell line under the identical cell culture conditions. The compound was excited at 860 nm and emission was recorded between 500-670 nm.

Two-photon imaging

Two-photon imaging used a custom-built multiphoton imaging system at Weill Cornell Medical College. The system consists of an Olympus BX61 upright microscope and a BioRad 1024 scan head. The specimens were excited using a tunable Ti-Sapphire laser (Mai Tai, Spectra-Physics) tuned to 860 nm. The laser power under the objective is controlled through a Pockel Cell (Conoptics). To avoid one photon process, 860 nm excitation light was used and the emitted light collected was between 500-670 nm. Note that the lowest energy optical absorption bands for the compounds in aqueous media are: $PGlc_4$ 645 nm, $CGlc_4$ 649 nm, $IGlc_4$ 645 nm, and $BGlc_4$ 730 nm. Thus, under these conditions, there is no single photon excitation of the compounds.

Two-photon cross section

2PA measurements were done as previously described (72). Briefly, a Ti–sapphire laser (Spectra-Physics Tsunami) pumped by a frequency doubled diode-pumped solid-state laser (Spectra-Physics Millennia) provided 90 fs pulses operating at 82 MHz was used to probe the 2PA properties of the dyes, and a CW (continuous wave) laser was used for the single photon studies. Both lasers were operated at the same power (6 mW). Experiments concerning quadratic dependence with the laser power were obtained using the femtosecond laser. Experiments were performed under the same conditions with rhodamine 6G as a standard and calculations used an existing protocol (73, 74).

Results and Discussion

The synthesis of $ChlF_{20}$(2), $IbacF_{20}$(3) and $BacF_{20}$(4) start from the commercially available $TPPF_{20}$(1) and cycloaddition reactions across pyrrole double bonds, as reported by Cavaleiro and coworkers.(69) The corresponding thioglycosylated conjugates, $PGlc_4$(5), $CGlc_4$(6), $IGlc_4$(7), and $BGlc_4$(8), are made by efficient nucleophilic substitution of the F group at the para position of the $TPPF_{20}$(20, 21, 23, 67). Other click-type reactions can yield glycosylated porphyrins (75). The reduction of pyrrolic double bonds and the methylpyrrolidine moiety used to stabilize the chlorin, isobacteriochlorin and bacteriochlorin may cause a deviation from the planarity compared to the $TPPF_{20}$ molecule, which may further change in the energy gap between HOMO and LUMO of the porphyrinoids. The classical four-orbital model developed by Gouterman account for the major optical features of the free base and metalloporphyrinoids in terms of transition between HOMO-LUMO (76). In addition to the rearrangement of the molecular orbitals due to the reduced double bonds, the red shift of the optical bands can also arise from the distorted macrocycle (77, 78).

UV-visible

The electronic spectra for the compounds $ChlF_{20}$, $IbacF_{20}$, $BacF_{20}$, $PGlc_4$, $CGlc_4$, $IGlc_4$, and $BGlc_4$ were recorded in three different solvents: ethyl acetate, ethanol, and phosphate buffered saline (PBS, pH=7.4) over the wavelength range of 300-900 nm (the upper limit of the instrument). UV-visible absorption spectra of compounds $ChlF_{20}$, $IbacF_{20}$, and $BacF_{20}$ in ethylacetate are shown in Figure 1. The UV-visible absorption spectra of $ChlF_{20}$, $IbacF_{20}$, and $BacF_{20}$ are slightly blue shifted from the corresponding thioglycosylated conjugates, $CGlc_4$, $IGlc_4$, and $BGlc_4$, and these are somewhat different from the porphyrin $TPPF_{20}$ and $PGlc_4$. The shift in the peaks may arise because of the change in the electronic environment with the substitution of electron withdrawing para F-atom on the meso substituted perfluorophenyl group by the electron donating S-atom of the thioglucose group. The Soret (B) bands for compounds $ChlF_{20}$, $IbacF_{20}$, and $BacF_{20}$ and $CGlc_4$, $IGlc_4$, and $BGlc_4$ broaden and are blue shifted. For compounds $IbacF_{20}$ and $IGlc_4$ the Soret band has two shoulders on the each side of the λ_{max}, while for compounds $BacF_{20}$ and $BGlc_4$ the Soret

band splits into two peaks. A significant increase in the absorption intensity of the lowest energy Q-band for conjugates $ChlF_{20}$, $IbacF_{20}$, and $BacF_{20}$ and $CGlc_4$, $IGlc_4$, and $BGlc_4$ were observed compare to the parent porphyrins $TPPF_{20}$ and $PGlc_4$. The lower energy Q-band for $ChlF_{20}$ and $CGlc_4$ at 649 nm in ethylacetate has about 25 fold greater intensity than the corresponding Q-band of $TPPF_{20}$ at 632 nm. For $IbacF_{20}$ and $IGlc_4$ a 25-fold increase in the absorption intensity was observed at 647 nm compared to $TPPF_{20}$ at 632 nm, while for $BacF_{20}$ and $BGlc_4$ the lowest energy Q-band is red shifted and appears at 730 nm with ca. 70-fold increased intensity compare to the absorption of $TPPF_{20}$ at 632 and $PGlc_4$ at 649 nm. For all of these compounds decomposition products such as dipyrrole methane or billirubin were not observed even upon exposure to ambient light. Also, there is no absorption peaks observed between 750-900 nm, in the area of two photon activity for the non-glycosylated $IbacF_{20}$ compound. UV-visible spectral data of compounds $ChlF_{20}$, $IbacF_{20}$, and $BacF_{20}$ in different solvents are summarized in Table 1 whereas for the spectra for compounds $PGlc_4$, $CGlc_4$, $IGlc_4$, and $BGlc_4$ were reported earlier by us (23) (See Supplementary Materials).

Fluorescence

The fluorescence emission spectra for compounds $ChlF_{20}$, $IbacF_{20}$, $BacF_{20}$, $PGlc_4$, $CGlc_4$, $IGlc_4$, and $BGlc_4$ were recorded in three different solvents: ethylacetate, ethanol and PBS and are found to have a strong solvent dependence. The emission peaks for compounds $ChlF_{20}$, $IbacF_{20}$, and $BacF_{20}$ are given in Table 1, whereas we reported the spectra for compounds $PGlc_4$, $CGlc_4$, $IGlc_4$, and $BGlc_4$(23) (see Supplementary Materials). Emission spectra of compounds $ChlF_{20}$, $IbacF_{20}$, and $BacF_{20}$ in ethylacetate are shown in Figure 2. There are negligible Stokes shifts observed for these conjugates in different solvents. The small Stokes shift for $PGlc_4$ and $CGlc_4$ in the three solvents likely indicates that most of the specific solvent-solute interactions are related to the sugar moieties. Notably, for the $IGlc_4$ in PBS, the strongest fluorescence band maxima are at 606 nm with a much weaker emission centered at 650 nm (see Supplementary Materials). Excitation spectra indicate the presence of only the given compounds. The fluorescence quantum yield for conjugates, $ChlF_{20}$, $IbacF_{20}$, $BacF_{20}$, $PGlc_4$, $CGlc_4$, $IGlc_4$, and $BGlc_4$ and in the above mentioned solvents are shown in Table 2. The 0.17 and 0.36 fluorescence quantum yields for $CGlc_4$ and for $IGlc_4$ in PBS are 6-fold and 12-fold greater than the porphyrin analogue $PGlc_4$. There is a small decrease in fluorescence quantum yield upon replacement of the para F-atom by the thioglucose due to both electronic and heavy atom effects. The greater fluorescence quantum yield of $CGlc_4$ compared to m-THPC ($\Phi = 0.09$ in methanol) (38), likely arises from the presence of the 16 F groups. Interestingly, the $BGlc_4$ system with the 730 nm absorption band has a fluorescence quantum yield of about 0.05 and thus for the present we assume most of the excited state intersystem crosses to the triplet manifold. Nonetheless, the fluorescence is sufficient to observe the uptake into cancer cell lines. Because $BGlc_4$ is a minor product, the smaller anti/syn ratio, and the set of diastereomers, this compound was not extensively evaluated. Our initial hypothesis was that the N- methylpyrrolidine moieties used to make and stabilize the chlorins, bacteriochlorins, and isobacteriochlorins would have minimal effect on cell uptake, because these are sandwiched between the phenyl-sugars; however there octanol/water partition coefficient range from ca. 10 for $IGlc_4$ and $BGlc_4$ to 30 for $CGlc_4$ and 40 for $PGlc_4$(23).

Excited state decay

The decay of the electron from the excited singlet state, S_1 to the ground singlet state, S_0 follows a series of radiative and/or non-radiative processes. The rate constant for these decay processes relates to the fluorescence quantum yield (Φ_f) and the fluorescence lifetime (τ_f) can be calculated using following equations:

$$\tau_f = 1/(k_f + k_{ic} + k_{isc}) \quad (1)$$

$$\Phi_f = k_f/(k_f + k_{ic} + k_{isc}) \quad (2)$$

k_f, k_{ic}, and k_{isc} are the rate constants for the radiative spontaneous fluorescence, internal conversion, and intersystem crossing to the triplet excited state, respectively. Using the above equations, the rate constant for non-radiative decay, k_{nr} is calculated (see Supplementary Materials). These compounds exhibit different degrees of excited state decay via radiative, non-radiative internal conversion, and $S_1 \rightarrow T_1$ intersystem crossing pathways that are also solvent dependent. A high fluorescence quantum yield indicates radiative $S_1 \rightarrow S_0$ decay dominates, whereas a low fluorescence quantum yield suggests decay is predominantly non-radiative via internal conversion and $S_1 \rightarrow T_1$(33, 41, 79). The greater Φ_f and radiative decay time constants, and low time constant for non-radiative decay for $CGlc_4$ and $IGlc_4$ indicate that these conjugates may serve as fluorescent tags. The low Φ_f, the 10-20 fold smaller radiative decay time constants, and the 2-fold greater non-radiative decay time constant for $PGlc_4$ and $BGlc_4$ indicates that these compounds enter the triplet manifold more efficiently, thus can serve as PDT agents.

The macrocycle distortion from the planarity and increased conformational dynamics causes the destabilization of the π-system and contributes to the significantly shorter lifetimes (80). This contributes to the ca. 2-4 fold shorter lifetimes for nonplanar glycosylated conjugates compared to the planar $TPPF_{20}$ compound.

The glycosylated derivatives are used to evaluate uptake by K:Molv NIH 3T3 mouse fibroblasts cells, vide infra. Ethylacetate, PBS, methanol or ethanol solvents were used to probe the photophysical properties since the amphipathic glycoporphyrinoids may localize in aqueous, highly polar, or hydrophobic environments within cells. The electronic spectra, fluorescence, and fluorescence microscopy studies all show that these compounds are robust to photobleaching (Figure 3). The remaining 16 F groups impart stability toward oxidative damage to the macrocycle and further enhance the photonic properties. The significantly greater fluorescence quantum yield of the $IGlc_4$ system indicates that it can be used at <25 nM concentrations in fluorescence microscopy. For PDT applications, sensitizers with strong red absorptions are generally considered better because these wavelengths penetrate deeper into tissue. The optical cross section of $CGlc_4$ in the red region is significantly larger than the porphyrin or isobacteriochlorin analogues. Thus, if red light is used to activate the $CGlc_4$ dye, the increased light absorptivity more than compensates the reduced triplet quantum yield. The enhanced fluorescence quantum yield of $IGlc_4$ makes it better suited for tagging and sensor applications, whereas the very strong 730 nm absorption and the low fluorescence quantum yield of $BGlc_4$ indicates that this may be the best photosensitizer for PDT of the compounds described herein. The singlet oxygen quantum yields are reported in Table 3.

Photobleaching of CGlc4

K:Molv 3T3 NIH cells were incubated with $CGlc_4$ for 24 hours to a final concentration of 0.1 μM and were prepared for confocal microscopy as described in the experimental section. The excitation wavelength was selected 552 nm and the emission band filter was 578-700 nm. The images show almost no photobleaching for this compound (Figure. 3), thus indicating that this chromophore can also be a good imaging agent, whereas the commercially available tracker dyes used for imaging purposes photobleach quickly under the same conditions (81).

Two Photon Microscopy

Since the emission of $IGlc_4$ and $BGlc_4$ taken up by cells was observable by two-photon microscopy, we investigated these derivatives to quantify the two photon absorption properties. Similar to our previous studies on the $PGlc_4$ with MDA-MB-231, CHO cells were incubated overnight with $PGlc_4$, $CGlc_4$, or a 5:1 mixture of $IGlc_4$ and $BGlc_4$ at 10 μM. Only the 5:1 mixture of $IGlc_4$ and $BGlc_4$ is observable with two photon microscopy, or at least, some fluorescence light in the range of 500 nm to 670 nm is detected when the compounds are excited with 860 nm light (Figure. 4). These results clearly show the possibility that either $IGlc_4$ or $BGlc_4$ has an appreciable two-photon cross section. In order to delineate the contributions of each compound to the observed two-photon microscopy images, the cells were incubated under the same conditions with $IbacF_{20}$ and $BacF_{20}$ separately. UV-visible spectra show that neither compound absorbs at the 860 nm excitation used in the two photon microscopy (Figure. 1). Since the fluorescence of $BacF_{20}$ begins around 720 nm and the detector is set up from 500 nm until 670 nm, significant fluorescence of this compound is not observed. The $IbacF_{20}$ is two-photon active (Figure. 5).

Two photon excitation

Although the one photon absorbance spectra of $IbacF_{20}$ and $BacF_{20}$ show no absorption peaks around 860 nm (Figure. 1), both compounds were excited using a continuous wave (CW) laser and a femtosecond (fs) laser to insure that the absorption process at this wavelength is due to a two photon process. The lower irradiance of the CW laser typically results in one photon excitation, while the fs laser can result in two photon excitation (72). The two photon efficiency depends on the instantaneous irradiance. The powers of both modes used here were the same.

Rhodamine 6G (R6G) was used as two photon reference to measure the two photon activity of $IbacF_{20}$ and $BacF_{20}$. The two photon reference, R6G, is not exited when the CW laser is used but is excited and fluorescence is measured when a fs laser is used. The fs pulse for $IbacF_{20}$, indicates that $IbacF_{20}$ is two photon active, and one photon absorption at 860 nm is not observed. Mixed results were obtained when $BacF_{20}$ is exited using a similar set up as one photon absorption can be observed when 760 nm, 780 nm or 800 nm wavelengths are used. Whereas at lower energy wavelengths (820 nm, 840 nm, 860 nm and 880 nm), both two photon and one photon absorption were observed (Supplementary Materials).

Two photon absorbance processes imply that the fluorescence emission increases quadratically with increasing laser power, rather than linearly for one photon emission. This behavior arises from the fact that two photons are absorbed in the same quantum event. With the fs laser, $BacF_{20}$, $IbacF_{20}$ and R6G were exited at 860 nm, and the fluorescence light measured as a function of laser power (Figure. 6). The observed combination of both absorption processes in the case of $BacF_{20}$ when laser excitation at 760 nm - 800 nm likely arises from the small but long tail of the lower energy absorption peak λ_{max} 730 nm, or there is a very small band centered at ca. 830 nm. An anti-Stokes effect is also possible wherein the molecule gets vibrational and rotational excitation from the basal level from kt energy, thus allowing excitation of the molecule with a lower energy than normally expected. Neither the small tail or the absorption band, nor the anti-Stokes effect is observed with the $IbacF_{20}$ compound because its lowest energy absorption peak λ_{max} at 600 nm is far away from the 760 nm laser. Thus $IbacF_{20}$ can only have a 2PA at wavelengths greater than 760 nm (Table 4).

Emission from $IbacF_{20}$ has a clear quadratic dependence on the laser power that is similar to the R6G standard while $BacF_{20}$ shows a linear dependence on the laser power (Figure. 6). These results confirm that $IbacF_{20}$ is indeed 2-photon active, and that $BacF_{20}$ either has little

or no two photon absorption (2PA) or the single photon processes dominate the observed fluorescence.

Two photon cross sections are difficult to measure consistently and accurately because of the large flux of photons needed from the fs laser can vary significantly. For this reason, all the 2PA calculations are based on the fluorescence light emitted when the sample is excited and by assuming this is directly proportional to the photons absorbed. This also assumes that the quantum yields of both reference and the sample are constant as a function of the wavelength. The reference for 2PA is R6G in methanol at 110 μM (quantum yield = 0.93). $IbacF_{20}$ was dissolved in DMSO at the same concentration (quantum yield = 0.15). The cross section (σ) of $IbacF_{20}$ was calculated for each wavelength using the following equation:

$$\sigma S(\lambda) = \frac{F(\lambda) \times QYr \times nr}{Fr(\lambda) \times QY \times n} \sigma \mathrm{r}(\lambda)$$

Where F(λ), Fr(λ), QY, QYr, σs(λ) and σr(λ) are the two photon fluorescence of the sample, two photon fluorescence of the reference, quantum yield of sample, quantum yield of the reference, sample cross section, and the reference cross section respectively, n_r and *n* are the refractive index of the solvents. The cross sections obtained are expressed in Table 4. Two-photon cross-sections for molecular systems are expressed in Goeppert-Mayer (GM) units, where 1 GM is 10^{-50} cm^4 s $photon^{-1}$.

Two photon photobleaching of IbacF20 in cells

The photo stability of the fluorescent imaging agent and/or PDT photosensitizer is very important, since longer photo stability would allow imaging over a greater amount of time or multiple images to be taken, and from a therapeutic perspective, the stability of the sensitizer to photo bleaching increases the efficacy of the dye.

To investigate the photo stability of $IbacF_{20}$, the compound was incubated into K:Molv NIH 3T3 cells. After 24 hours the cells were washed 3 times with PBS buffer. 25 scans were performed using the two photon microscope and the first image from the first scan was compared to the last image from the last scan. As shown in Figure 7, $IbacF_{20}$ does not significantly photobleach. Thus this core platform may be an excellent choice for both therapeutic and imaging applications where one needs to follow cells or biochemical processes over time. The photo stability of $IGlc_4$ and $CGlc_4$ was also measured in sunlight on sunny days wherein 1 μM solution of the conjugates in ethanol were exposed to sunlight and UV-visible spectra were recorded versus time for 3-4 hours (see Supplementary Materials). Photobleaching was observed for $CGlc_4$ ca. 5%, for $IGlc_4$ ca. 10%,, and we reported previously ca. 10% for $IGlc_4$(23).

Bioimaging

Head and neck squamous carcinoma (HNSCC) tumors indicate a poor long-term prognosis. Single photon fluorescence imaging investigations were made to determine the uptake of the glycosylated compounds into HNSCC in mouse models. Subcutaneous injection of athymic mice with a HNSCC cell line expressing green fluorescent protein (GFP) results in tumors that can be tracked by fluorescence imaging. When tumors reached adequate size 100 μL of 5 mg/mL solution of $PGlc_4$ or $IGlc_4$ or $CGlc_4$ in PBS was injected in tail vein of the mouse (50). Fluorescence images were collected periodically using different band pass filters to distinguish GFP versus dye emission (Figure. 8). This series of whole mouse images

indicates some accumulation of the $IGlc_4$ and $CGlc_4$ in the xenograft tumor. $IGlc_4$ fluorescence was initially observed in the mouse brain, spinal column, and liver five minutes after the tail vein injection, and a maximum $IGlc_4$ fluorescence was detected in the xenograft tumors after 30 minutes injection. The $IGlc_4$ fluorescence indicates the dye was cleared in ca. 21 hours after injection. $CGlc_4$ distribution was significantly delayed compared to $IGlc_4$ in that that the fluorescence was initially detected in xenograft tumors, brain and liver 21 hours after injection. Interestingly, a large amount of $CGlc_4$ fluorescence was accumulated in the xenograft tumors 24 hours after injection. $PGlc_4$ does not yield consistent results under these conditions, which is likely due to the low fluorescence quantum yield and perhaps because the dyes remain aggregated for a longer time in the mice. Mice were monitored an additional 21 days to assess the effects of $IGlc_4$, $CGlc_4$ and $PGlc_4$ on the xenograft tumor growth. Both $CGlc_4$ and $PGlc_4$ showed a notable capacity to inhibit xenograft tumor growth under the standard conditions for keeping mice, i.e. no specific light irradiation of the tumors. The tumor weight in $CGlc_4$ or $PGlc_4$ treated groups was approximately 24% to 34% lower than untreated control groups (Figure. 9). This may indicate some effect of the compound under the ambient light used to keep the mice. Though the $^1O_2\Phi_\Delta$ of 0.59 is greater than for $CGlc_4$, there was no statistically significant difference of tumor weight between $IGlc_4$ treated and untreated groups, which may result from the faster pharmacokinetics.

Conclusion

Since nucleophilic aromatic substitution of the para fluoro group is rapid and efficient, these studies provide the methods to synthesize and evaluate a wide range of exocyclic motifs for applications ranging from photonic materials to therapeutics (67). Amphipathic compounds such as these glycosylated dyes are often found to be more effective PDT agents (82, 83). Both $CGlc_4$ and $IGlc_4$ have significantly enhanced fluorescence quantum yields compared to the $PGlc_4$, while the $BGlc_4$ derivative has a fluorescence quantum yield that is similar to the parent porphyrin. Thus $IGlc_4$ has greatest potential use as fluorescent tags, diagnostics, or imaging agents. The intermediate fluorescence of the $CGlc_4$ system may well serve as a theragnostic agent for targeting, detecting, and treating diseased tissues. The $BGlc_4$ system has near optimal properties as the PDT agent, but new synthetic strategies are needed to make these compounds. The much lower concentrations of $CGlc_4$ and $IGlc_4$ needed for fluorescence microscopy indicate these compounds can be used as bioimaging and diagnostic tools. $IbacF_{20}$ has 2PA between 760 nm to 880 nm, while $BacF_{20}$ is largely a one photon dye that may have small contributions from two photon processes. Both the compounds have advantages compared to currently used photosensitizers for PDT: (a) strong red light absorbance, (b) the exocyclic glucose moieties target cancer cells over normal cells. The 2PA properties of $IbacF_{20}$, while not large compared to the multichromophore systems reported, are sufficient for imaging applications and perhaps for therapeutic applications. The role of aggregation and possible differences in metabolism in vivo is under investigation.

Supplementary Material

Refer to Web version on PubMed Central for supplementary material.

Acknowledgments

We thanks Dr. Tymish Y. Ohulchanskyy of the Institute of Photomedicine, State University of New York at Buffalo for help in determining the 2-photon cross section. supported by the U.S. National Science Foundation (NSF CHE-0847997 and 1213962 to CMD, and Hunter College science infrastructure is supported by the NSF, including the National Institute on Minority Health and Health Disparities (8G12 MD007599) and the City

University of New York. The RCMI/NIMHD program (8G12 MD007597) at Howard University and The RTRN/NIMHD program (U54MD008149).

References

1. Kadish, K.; Smith, K.; Guilard, R. The Handbook of Porphyrin Science with Applications to Chemistry, Physics, Materials Science, Engineering, Biology and Medicine. World Scientific Publishers; Singapore: 2010.
2. Bonnett R. Photosensitizers of the porphyrin the phthalocyanine series for phtodynamic therapy. Chem Soc Rev. 1995; 24:19–33.
3. Pandey RK. Recent advances in photodynamic therapy. J Porphyrins Phthalocyanines. 2000; 4:368–373.
4. Sternberg ED, Dolphin D, Brückner C. Porphyrin-based photosensitizers for use in photodynamic therapy. Tetrahedron. 1998; 54:4151–4202.
5. Lovell JF, Liu TWB, Chen J, Zheng G. Activatable Photosensitizers for Imaging and Therapy. Chem Rev. 2010; 110:2839–2857. [PubMed: 20104890]
6. Allison RR, Downie GH, Cuenca R, Hu XH, Childs CJH, Sibata CH. Photosensitizers in clinical PDT. Photodiag Photodyn Ther. 2004; 1:27–42.
7. Agostinis P, Berg K, Cengel KA, Foster TH, Girotti AW, Gollnick SO, Hahn SM, Hamblin MR, Juzeniene A, Kessel D, Korbelik M, Moan J, Mroz P, Nowis D, Piette J, Wilson BC, Golab J. Photodynamic therapy of cancer: An update. CA- Cancer J Clin. 2011; 61:250–281. [PubMed: 21617154]
8. Pushpan SK, Venkatraman S, Anand VG, Sankar J, Parmeswaran D, Ganesan S, Chandrashekar TK. Porphyrins in Photodynamic Therapy - A Search for Ideal Photosensitizers. Curr Med Chem - Anti-Cancer Agents. 2002; 2:187–207.
9. Ethirajan M, Chen Y, Joshi P, Pandey RK. The role of porphyrin chemistry in tumor imaging and photodynamic therapy. Chem Soc Rev. 2011; 40:340–362. [PubMed: 20694259]
10. Spikes JD. New trends in photobiology: Chlorins as photosensitizers in biology and medicine. J Photochem Photobiol B: Biol. 1990; 6:259–274.
11. Senge MO, Brandt JC. Temoporfin (Foscan®, 5,10,15,20-Tetra(m-hydroxyphenyl)chlorin)—A second-generation photosensitizer. Photochem Photobiol. 2011; 87:1240–1296. [PubMed: 21848905]
12. Arnaut, LG. Design of porphyrin-based photosensitizers for photodynamic therapy. In: Rudi van, E.; Grażyna, S., editors. Adv Inorg Chem. Vol. 63. Academic Press; 2011. p. 187-233.
13. Ambrosi M, Cameron NR, Davis BG. Lectins: tools for the molecular understanding of the glycocode. Org Biomol Chem. 2005; 3:1593–1608. [PubMed: 15858635]
14. Dwek RA. Glycobiology: Toward Understanding the Function of Sugars. Chem Rev. 1996; 96:683–720. [PubMed: 11848770]
15. Monsigny M, Roche AC, Kieda C, Midoux P, Obrenovitch A. characterization and biological implications of membrane lectins in tumor, lymphoid and myloid cells. Biochimie. 1988; 70:1633–1649. [PubMed: 3149528]
16. Gorelik E, Galili U, Raz A. On the Role of Cell Surface Carbohydrates and their Binding Proteins (lectins) in Tumor Metastasis. Cancer Metastasis Rev. 2001; 20:245–277. [PubMed: 12085965]
17. Warburg O. On the Origin of Cancer Cells. Science. 1956; 123:309–314. [PubMed: 13298683]
18. Kim JW, Dang CV. Cancer's Molecular Sweet Tooth and the Warburg Effect. Cancer Res. 2006; 66:8927–8930. [PubMed: 16982728]
19. Ballut S, Naud-Martin D, Loock B, Maillard P. A Strategy for the Targeting of Photosensitizers. Synthesis, Characterization, and Photobiological Property of Porphyrins Bearing Glycodendrimeric Moieties. J Org Chem. 2011; 76:2010–2028. [PubMed: 21361314]
20. Pasetto P, Chen X, Drain CM, Franck RW. Synthesis of hydrolytically stable porphyrin - and -glycoconjugates in high yields. Chem Commun. 2001:81–82.
21. Chen X, Hui L, Foster DA, Drain CM. Efficient Synthesis and Photodynamic Activity of Porphyrin-Saccharide Conjugates: Targeting and Incapacitating Cancer Cells. Biochem. 2004; 43:10918–10929. [PubMed: 15323552]

22. Chen, X.; Drain, CM. Drug Design Rev - Online. Vol. 1. Bentham Science Publishers Ltd; 2004. Photodynamic Therapy Using Carbohydrate Conjugated Porphyrins; p. 215-234.
23. Singh S, Aggarwal A, Thompson S, Tomé JPC, Zhu X, Samaroo D, Vinodu M, Gao R, Drain CM. Synthesis and Photophysical Properties of Thioglycosylated Chlorins, Isobacteriochlorins, and Bacteriochlorins for Bioimaging and Diagnostics. Bioconjugate Chem. 2010; 21:2136–2146.
24. Drain CM, Singh S, Samaroo D, Thompson S, Vinodu M, Tome JPC. New Porphyrin Glyco-conjugates. Proc Soc Photo-Optical Instrument Engin-SPIE. 2009; 7380:73902K-1–9.
25. Kadish, KM.; Smith, KM.; Guilard, R. The Porphyrin Handbook: Synthesis and organic chemistry. Vol. 1. Academic Press; San Diego: 2000.
26. Lim SH, Lee HB, Ho ASH. A New Naturally Derived Photosensitizer and Its Phototoxicity on Head and Neck Cancer Cells. Photochem Photobiol. 2011; 87:1152–1158. [PubMed: 21534974]
27. Mauzerall DC. Evolution of Porphyrins. Clinic Dermatology. 1998; 16:195–201.
28. Gouterman M. Spectra of porphyrins. J Mol Spect. 1961; 6:138–163.
29. Ghosh A. First-Principles Quantum Chemical Studies of Porphyrins. Acc Chem Res. 1998; 31:189–198.
30. Yang E, Kirmaier C, Krayer M, Taniguchi M, Kim HJ, Diers JR, Bocian DF, Lindsey JS, Holten D. Photophysical Properties and Electronic Structure of Stable, Tunable Synthetic Bacteriochlorins: Extending the Features of Native Photosynthetic Pigments. J Phys Chem B. 2011; 115:10801–10816. [PubMed: 21875047]
31. Taniguchi M, Cramer DL, Bhise AD, Kee HL, Bocian DF, Holten D, Lindsey JS. Accessing the Near-Infrared Spectral Region with Stable, Synthetic, Wavelength-tunable Bacteriochlorins. New J Chem. 2008; 32:947–958.
32. Drain, CM.; Singh, S. Combinatorial Chemistry of Porphyrins. In: Kadish, R.; Guilard, R.; Smith, K., editors. The Handbook of Porphyrin Science with Applications to Chemistry, Physics, Materials Science, Engineering, Biology and Medicine. Vol. 2. World Scientific; Singapore: 2010. p. 485-540.
33. Kee HL, Bhaumik J, Diers JR, Mroz P, Hamblin MR, Bocian DF, Lindsey JS, Holten D. Photophysical characterization of imidazolium-substituted Pd(II), In(III), and Zn(II) porphyrins as photosensitizers for photodynamic therapy. J Photochem Photobiol A: Chem. 2008; 200:346–355. [PubMed: 20016663]
34. Hirohara S, Obata M, Alitomo H, Sharyo K, Ando T, Yano S, Tanihara M. Synthesis and Photocytotoxicity of S-Glucosylated 5,10,15,20-Tetrakis(tetrafluorophenyl)porphyrin Metal Complexes as Efficient $^1O_2$-Generating Glycoconjugates. Bioconjugate Chem. 2009; 20:944–952.
35. Hirohara S, Obata M, Alitomo H, Sharyo K, Ogata Si, Ohtsuki C, Yano S, Ando T, Tanihara M. Structure and Photodynamic Effect Relationships of 24 Glycoconjugated Photosensitizers in HeLa Cells. Biol Pharm Bull. 2008; 31:2265–2272. [PubMed: 19043211]
36. Drain CM, Gentemann S, Roberts JA, Nelson NY, Medforth CJ, Jia SL, Simpson MC, Smith KM, Fajer J, Shelnutt JA, Holten D. Picosecond to microsecond photodynamics of a nonplanar nickel porphyrin: Solvent dielectric and temperature effects. J Am Chem Soc. 1998; 120:3781–3791.
37. Drain CM, Kirmaier C, Medforth CJ, Nurco J, Smith KM, Holten D. Dynamic photophysical properties of conformationally distorted nickel porphyrins .1. Nickel(II) dodecaphenylporphyrin. J Phys Chem. 1996; 100:11984–11993.
38. Bonnett R, Charlesworth P, Djelal BD, Foley S, McGarvey DJ, George Truscott T. Photophysical properties of 5,10,15,20-tetrakis(m-hydroxyphenyl)porphyrin (m-THPP), 5,10,15,20-tetrakis(m-hydroxyphenyl)chlorin (m-THPC) and 5,10,15,20-tetrakis(m-hydroxyphenyl)bacteriochlorin (m-THPBC): a comparative study. J Chem Soc Perkin Trans. 1999; 2:325–328.
39. Laville I, Figueiredo T, Loock B, Pigaglio S, Maillard P, Grierson DS, Carrez D, Croisy A, Blais J. Synthesis, cellular internalization and photodynamic activity of glucoconjugated derivatives of tri and tetra(meta-hydroxyphenyl)chlorins. Bioorg Med Chem. 2003; 11:1643–1652. [PubMed: 12659750]
40. Silva AMG, Tomé AC, Neves MGPMS, Silva AMS, Cavaleiro JAS, Perrone D, Dondoni A. Porphyrins in 1,3-dipolar cycloaddition reactions with sugar nitrones. Synthesis of glycoconjugated isoxazolidine-fused chlorins and bacteriochlorins. Tet Lett. 2002; 43:603–605.

41. Huang YY, Mroz P, Zhiyentayev T, Sharma SK, Balasubramanian T, Ruzié C, Krayer M, Fan D, Borbas KE, Yang E, Kee HL, Kirmaier C, Diers JR, Bocian DF, Holten D, Lindsey JS, Hamblin MR. In Vitro Photodynamic Therapy and Quantitative Structure–Activity Relationship Studies with Stable Synthetic Near-Infrared-Absorbing Bacteriochlorin Photosensitizers. J Med Chem. 2010; 53:4018–4027. [PubMed: 20441223]

42. McCarthy JR, Bhaumik J, Merbouh N, Weissleder R. High-yielding syntheses of hydrophilic conjugatable chlorins and bacteriochlorins. Org Biomol Chem. 2009; 7:3430–3436. [PubMed: 19675897]

43. Yang E, Ruzié C, Krayer M, Diers JR, Niedzwiedzki DM, Kirmaier C, Lindsey JS, Bocian DF, Holten D. Photophysical Properties and Electronic Structure of Bacteriochlorin–Chalcones with Extended Near-Infrared Absorption. Photochem Photobiol. 2013; 89:586–604. [PubMed: 23360219]

44. Silva JN, Silva AMG, Tome JP, Ribeiro AO, Domingues MRM, Cavaleiro JAS, Silva AMS, Graca M, Neves M, Tome AC, Serra OA, Bosca F, Filipe P, Santuse R, Morliere P. Photophysical properties of a photocytotoxic fluorinated chlorin conjugated to four β-cyclodextrins. Photochem Photobiol Sci. 2008; 7:834–843. [PubMed: 18597032]

45. Drobizhev M, Karotki A, Kruk M, Rebane A. Resonance enhancement of two-photon absorption in porphyrins. Chem Phys Lett. 2002; 355:175–182.

46. Hänninen P, Soukka J, Soini JT. Two-photon Excitation Fluorescence Bioassays. Ann NY Acad Sci. 2008; 1130:320–326. [PubMed: 18596366]

47. Garcia G, Hammerer F, Poyer F, Achelle S, Teulade-Fichou MP, Maillard P. Carbohydrate-conjugated porphyrin dimers: Synthesis and photobiological evaluation for a potential application in one-photon and two-photon photodynamic therapy. Bioorg Med Chem. 2013; 21:153–165. [PubMed: 23218779]

48. Dy J, Ogawa K, Satake A, Ishizumi A, Kobuke Y. Water-Soluble Self-Assembled Butadiyne-Bridged Bisporphyrin: A Potential Two-Photon-Absorbing Photosensitizer for Photodynamic Therapy. Chem Eur J. 2007; 13:3491–3500. [PubMed: 17225219]

49. Diaspro A, Chirico G, Collini M. Two-photon fluorescence excitation and related techniques in biological microscopy. Quarterly Rev Biophys. 2005; 38:97–166.

50. Rubart M. Two-Photon Microscopy of Cells and Tissue. Circulation Res. 2004; 95:1154–1166. [PubMed: 15591237]

51. Mir Y, van Lier JE, Allard JF, Morris D, Houde D. Two-photon absorption cross section of excited phthalocyanines by a femtosecond Ti-sapphire laser. Photochem Photobiol Sci. 2009; 8:391–395. [PubMed: 19255681]

52. Drobizhev M, Meng F, Rebane A, Stepanenko Y, Nickel E, Spangler CW. Strong Two-Photon Absorption in New Asymmetrically Substituted Porphyrins: Interference between Charge-Transfer and Intermediate-Resonance Pathways. J Phys Chem B. 2006; 110:9802–9814. [PubMed: 16706432]

53. Starkey JR, Rebane AK, Drobizhev MA, Meng F, Gong A, Elliott A, McInnerney K, Spangler CW. New Two-Photon Activated Photodynamic Therapy Sensitizers Induce Xenograft Tumor Regressions after Near-IR Laser Treatment through the Body of the Host Mouse. Clin Cancer Res. 2008; 14:6564–6573. [PubMed: 18927297]

54. Dichtel WR, Serin JM, Edder C, Fréchet JMJ, Matuszewski M, Tan LS, Ohulchanskyy TY, Prasad PN. Singlet Oxygen Generation via Two-Photon Excited FRET. J Am Chem Soc. 2004; 126:5380–5381. [PubMed: 15113208]

55. Balaz M, Collins HA, Dahlstedt E, Anderson HL. Synthesis of hydrophilic conjugated porphyrin dimers for one-photon and two-photon photodynamic therapy at NIR wavelengths. Org Biomol Chem. 2009; 7:874–888. [PubMed: 19225670]

56. Dahlstedt E, Collins HA, Balaz M, Kuimova MK, Khurana M, Wilson BC, Phillips D, Anderson HL. One- and two-photon activated phototoxicity of conjugated porphyrin dimers with high two-photon absorption cross sections. Org Biomol Chem. 2009; 7:897–904. [PubMed: 19225672]

57. Kuimova MK, Collins HA, Balaz M, Dahlstedt E, Levitt JA, Sergent N, Suhling K, Drobizhev M, Makarov NS, Rebane A, Anderson HL, Phillips D. Photophysical properties and intracellular

imaging of water-soluble porphyrin dimers for two-photon excited photodynamic therapy. Org Biomol Chem. 2009; 7:889–896. [PubMed: 19225671]

58. Drobizhev M, Stepanenko Y, Rebane A, Wilson CJ, Screen TEO, Anderson HL. Strong Cooperative Enhancement of Two-Photon Absorption in Double-Strand Conjugated Porphyrin Ladder Arrays. J Am Chem Soc. 2006; 128:12432–12433. [PubMed: 16984190]
59. Easwaramoorthi S, Jang SY, Yoon ZS, Lim JM, Lee CW, Mai CL, Liu YC, Yeh CY, Vura-Weis J, Wasielewski MR, Kim D. Structure–Property Relationship for Two-Photon Absorbing Multiporphyrins: Supramolecular Assembly of Highly-Conjugated Multiporphyrinic Ladders and Prisms. J Phys Chem A. 2008; 112:6563–6570. [PubMed: 18588270]
60. Biswas S, Ahn HY, Bondar MV, Belfield KD. Two-Photon Absorption Enhancement of Polymer-Templated Porphyrin-Based J-Aggregates. Langmuir. 2011; 28:1515–1522. [PubMed: 22188399]
61. Collini E, Ferrante C, Bozio R. Influence of Excitonic Interactions on the Transient Absorption and Two-Photon Absorption Spectra of Porphyrin J-Aggregates in the NIR Region. J Phys Chem C. 2007; 111:18636–18645.
62. Achelle S, Couleaud P, Baldeck P, Teulade-Fichou MP, Maillard P. Carbohydrate–Porphyrin Conjugates with Two-Photon Absorption Properties as Potential Photosensitizing Agents for Photodynamic Therapy. Eur J Org Chem. 2011; 2011:1271–1279.
63. Hammerer F, Achelle S, Baldeck P, Maillard P, Teulade-Fichou MP. Influence of Carbohydrate Biological Vectors on the Two-Photon Resonance of Porphyrin Oligomers. J Phys Chem A. 2011; 115:6503–6508. [PubMed: 21585209]
64. Ogawa K, Hasegawa H, Inaba Y, Kobuke Y, Inouye H, Kanemitsu Y, Kohno E, Hirano T, Ogura Si, Okura I. Water-Soluble Bis(imidazolylporphyrin) Self-Assemblies with Large Two-Photon Absorption Cross Sections as Potential Agents for Photodynamic Therapy. J Med Chem. 2006; 49:2276–2283. [PubMed: 16570924]
65. Fisher JAN, Susumu K, Therien MJ, Yodh AG. One- and two-photon absorption of highly conjugated multiporphyrin systems in the two-photon Soret transition region. J Chem Phys. 2009; 130:134506–8. [PubMed: 19355750]
66. Samaroo D, Vinodu M, Chen X, Drain CM. meso-Tetra(pentafluorophenyl) porphyrin as an Efficient Platform for Combinatorial Synthesis and the Selection of New Photodynamic Therapeutics using a Cancer Cell Line. J Comb Chem. 2007; 9:998–1011. [PubMed: 17877415]
67. Drain, CM.; Singh, S. Combinatorial libraries of porphyrins: Chemistry and applications. In: Kadish, K.; Smith, KM.; Guilard, R., editors. The Handbook of Porphyrin Science with Applications to Chemistry, Physics, Materials Science, Engineering, Biology and Medicine. Vol. 1. World Scientific Publisher; Singapore: 2010.
68. Thompson S, Chen X, Hui L, Toschi A, Foster DA, Drain CM. Low concentrations of a non-hydrolysable tetra-S-glycosylated porphyrin and low light induces apoptosis in human breast cancer cells via stress of the endoplasmic reticulum. Photochem Photobiol Sci. 2008; 7:1415–1421. [PubMed: 18958330]
69. Silva AMG, Tomé AC, Neves MGPMS, Silva AMS, Cavaleiro JAS. 1,3-Dipolar Cycloaddition Reactions of Porphyrins with Azomethine Ylides. J Org Chem. 2005; 70:2306–2314. [PubMed: 15760219]
70. Seybold PG, Gouterman M. Porphyrins: XIII: Fluorescence spectra and quantum yields. J Mol Spectrosc. 1969; 31:1–13.
71. Bonnett R, Martínez G. Photobleaching of sensitisers used in photodynamic therapy. Tetrahedron. 2001; 57:9513–9547.
72. Khurana M, Collins HA, Karotki A, Anderson HL, Cramb DT, Wilson BC. Quantitative In Vitro Demonstration of Two-Photon Photodynamic Therapy Using Photofrin® and Visudyne®. Photochem Photobiol. 2007; 83:1441–1448. [PubMed: 18028219]
73. Xu C, Webb WW. Measurement of two-photon excitation cross sections of molecular fluorophores with data from 690 to 1050 nm. J Opt Soc Am B. 1996; 13:481–491.
74. Fischer M, Georges J. Fluorescence quantum yield of rhodamine 6G in ethanol as a function of concentration using thermal lens spectrometry. Chem Phys Lett. 1996; 260:115–118.

75. Grin MA, Lonin IS, Makarov AI, Lakhina AA, Toukach FV, Kachala VV, Orlova AV, Mironov AF. Synthesis of chlorin-carbohydrate conjugates by 'click chemistry'. Mendeleev Commun. 2008; 18:135–137.

76. Gouterman, M. The Porphyrins. Dolphin, D., editor. Vol. III. Academic Press; New York: 1978. p. 1

77. Drain CM, Gentemann S, Roberts JA, Nelson NY, Medforth CJ, Jia S, Simpson MC, Smith KM, Fajer J, Shelnutt JA, Holten D. Picosecond to Microsecond Photodynamics of a Nonplanar Nickel Porphyrin: Solvent Dielectric and Temperature Effects. J Am Chem Soc. 1998; 120:3781–3791.

78. Drain CM, Kirmaier C, Medforth CJ, Nurco DJ, Smith KM, Holten D. Dynamic Photophysical Properties of Conformationally Distorted Nickel Porphyrins. 1. Nickel(II) Dodecaphenylporphyrin. J Phys Chem. 1996; 100:11984–11993.

79. Muthiah, Chinnasamy; Taniguchi, Masahiko; Kim, Han-Je; Schmidt, Izabela; Kee, Hooi Ling; Holten, Dewey; Bocian, David F.; Lindsey, JS. Synthesis and Photophysical Characterization of Porphyrin, Chlorin and Bacteriochlorin Molecules Bearing Tethers for Surface Attachment. Photochem Photobiol. 2007; 83:1513–1528. [PubMed: 18028228]

80. Gentemann S, Medforth CJ, Forsyth TP, Nurco DJ, Smith KM, Fajer J, Holten D. Photophysical Properties of Conformationally Distorted Metal-Free Porphyrins. Investigation into the Deactivation Mechanisms of the Lowest Excited Singlet State. J Am Chem Soc. 1994; 116:7363–7368.

81. Cselenyák, A.; Pankotai, E.; Csordás, A.; Kiss, L.; Lacza, Z. Live-Cell Fluorescent Imaging of Membrane or Mitochondrion Transfer between Connected Cells in Culture. In: Méndez-Vilas, A.; Díaz, J., editors. Microscopy: Science, Technology, Applications and Education. Vol. 1. Formatex; Badajoz, Spain: 2010. p. 764-771.

82. Oulmi D, Maillard P, Guerquin-Kern JL, Huel C, Momenteau M. Glycoconjugated Porphyrins. 3. Synthesis of Flat Amphiphilic Mixed meso-(Glycosylated aryl)arylporphyrins and Mixed meso-(Glycosylated aryl)alkylporphyrins Bearing Some Mono- and Disaccharide Groups. J Org Chem. 1995; 60:1554–1564.

83. Laville I, Pigaglio S, Blais JC, Doz F, Loock B, Maillard P, Grierson DS, Blais J. J Med Chem. 2006; 49:2558–2567. [PubMed: 16610799]

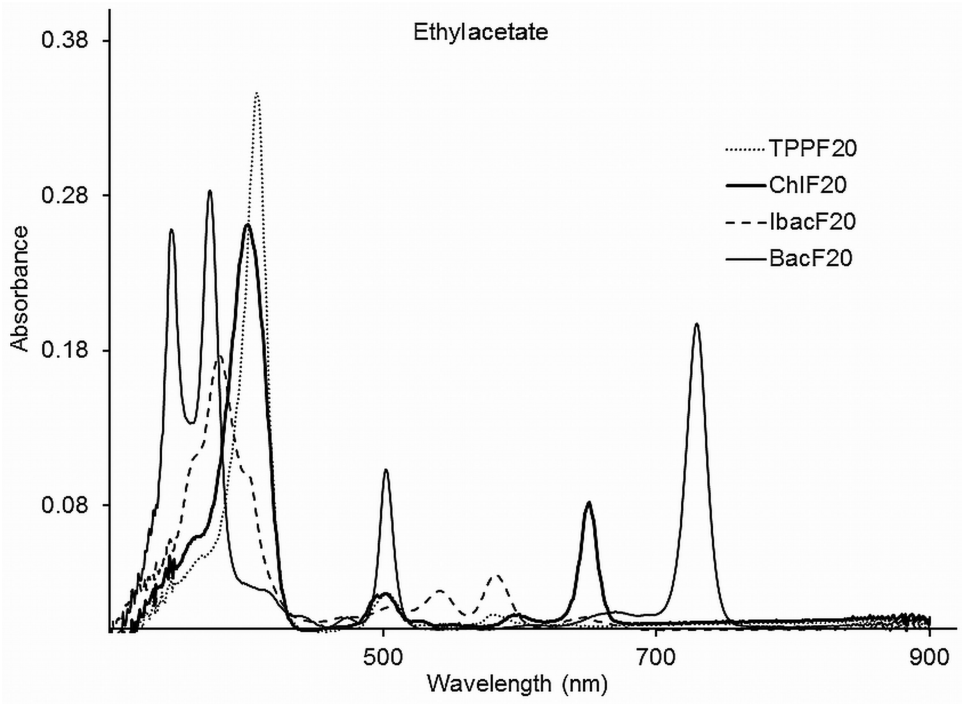

Figure 1.
UV-visible absorption spectra of compounds **1-4** in ethylacetate in 1 cm cuvettes and the concentration of each solution was 1 μM.

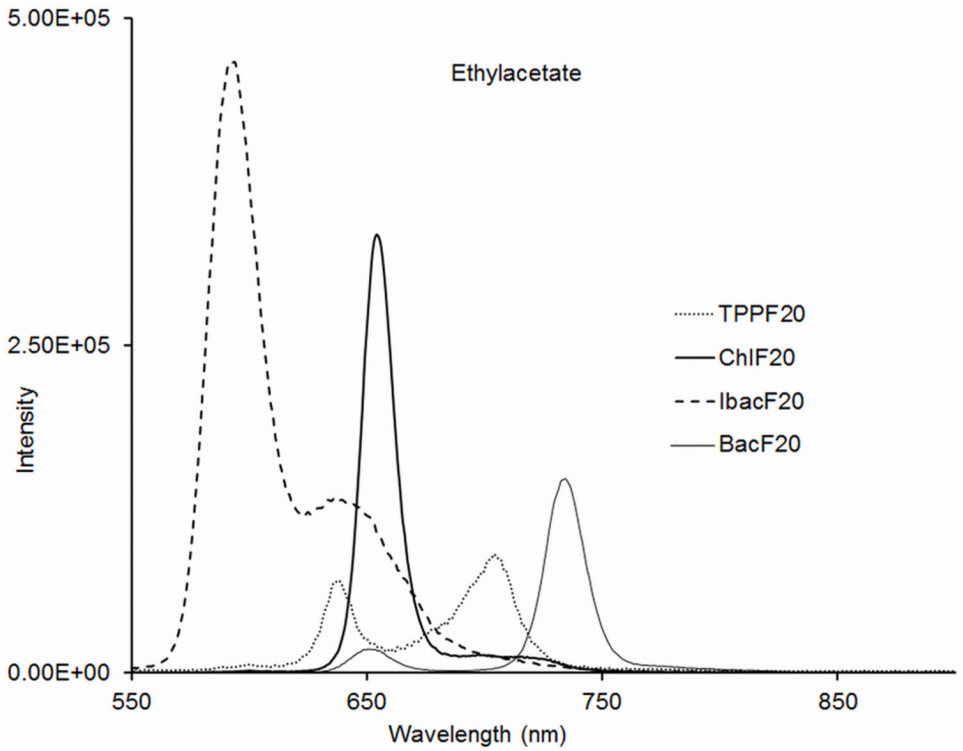

Figure 2.
Emission spectra of compounds **2-4** in ethylacetate; excitation at 509 nm where the O.D was 0.014 for each compound.

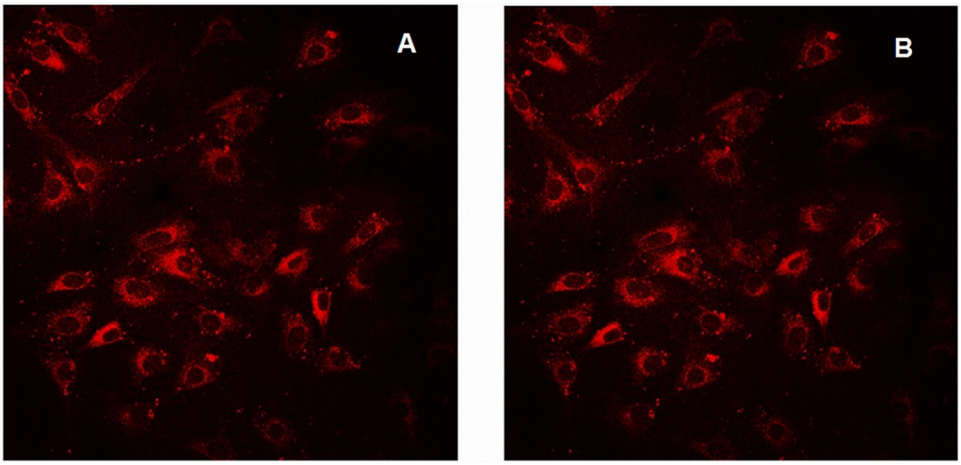

Figure 3.

K:Molv 3T3 NIH cells plated onto cover slips were incubated with $CGlc_4$ for 24 hours, washed three times with PBS buffer, fixed with 4% paraformaldehyde, again washed three times with PBS, and mounted in Dako fluorescence mounting medium. Confocal images were taken using excitation wavelength 552 nm and emission filter was 578-700 nm. A: image after first scan, and B: image of the same sample after 25 scans. The images are as collected.

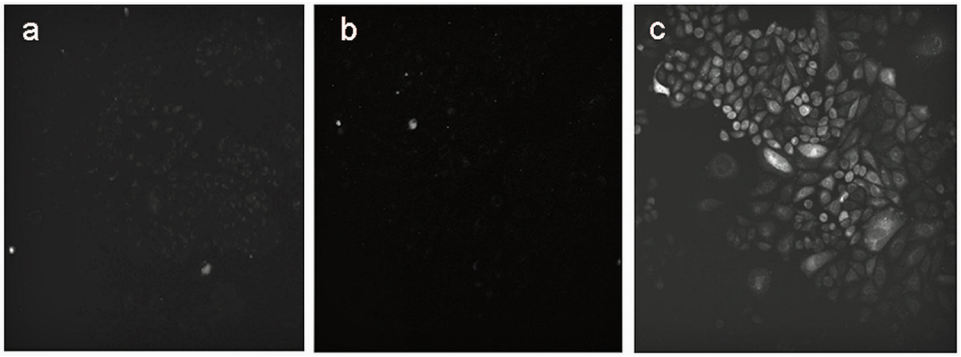

Figure 4.

CHO cells were incubated overnight with a) 10 μM $PGlc_4$ b) 10 μM $CGlc_4$ c) 10 μM of a mixture of $IGlc_4$: $BGlc_4$ (5:1). Two-photon microscope excitation light was at 860 nm, and the detector was set for 500 nm to 670 nm. The image data was collected for 1s. The images are as collected.

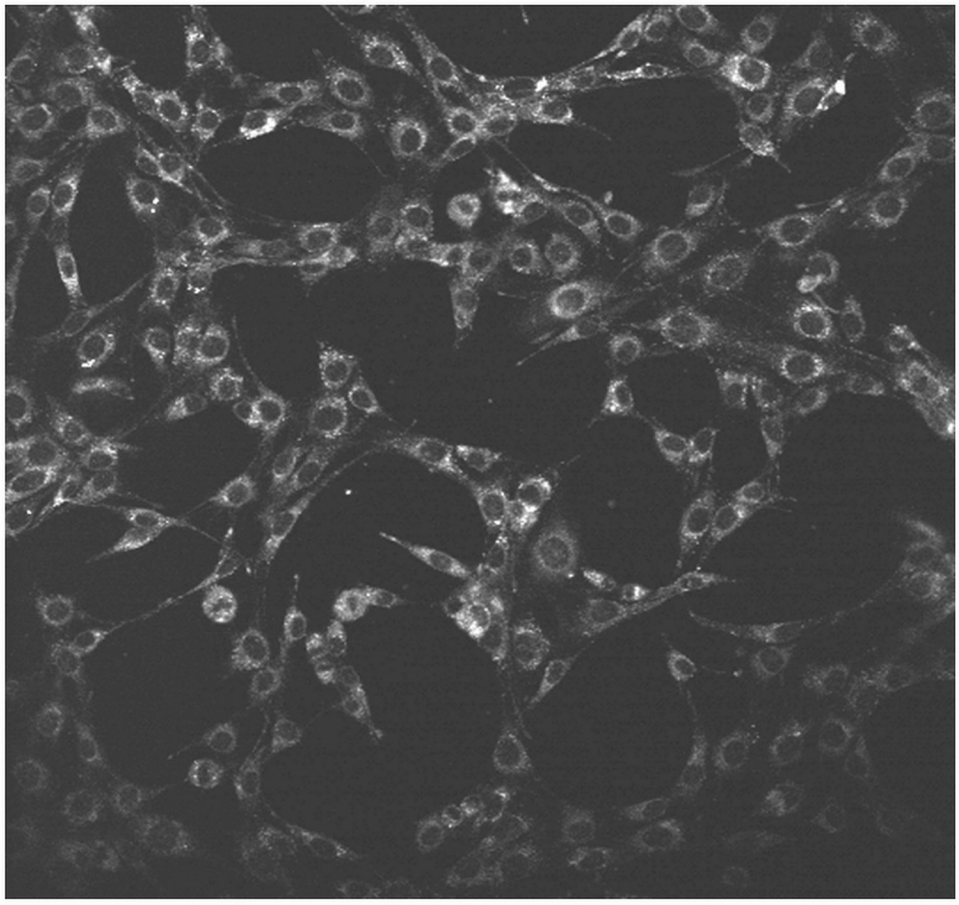

Figure 5.
K:Molv NIH 3T3 cells were incubated with 10 μM of $IbacF_{20}$ overnight. Two-photon microscope excitation light was at 860 nm, and the detector was set for 500 nm to 670 nm. The image data was collected for 1 s. The image is as collected.

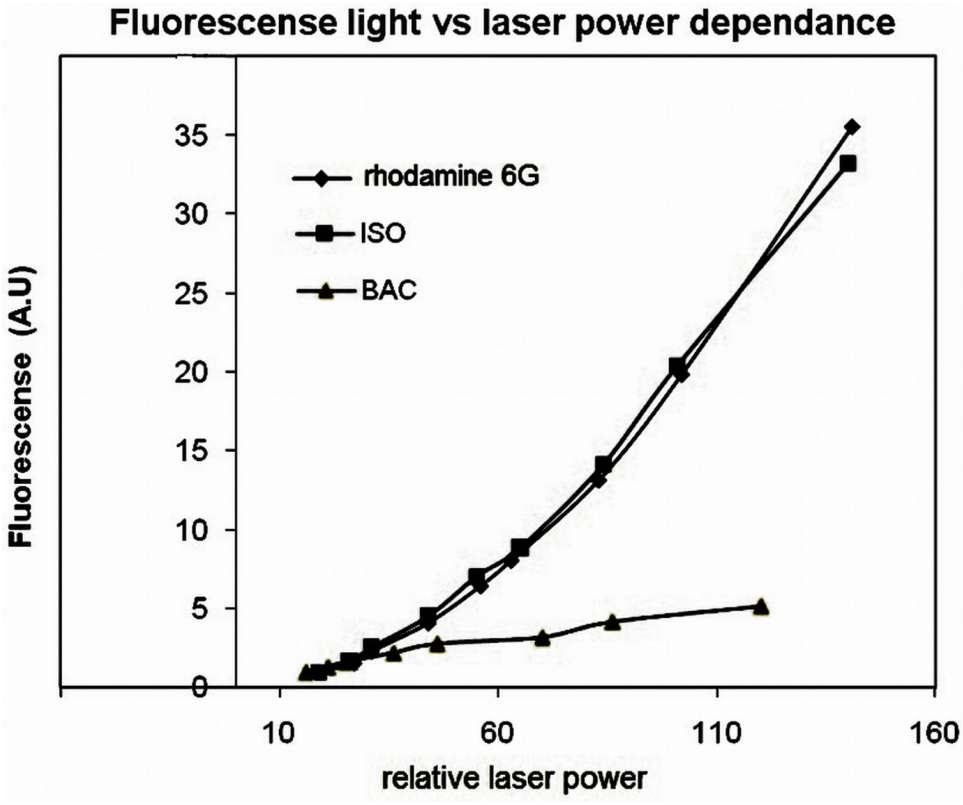

Figure 6.
Dependence of light emitted versus laser power. Excitation: 860 nm. Light collected: 500 nm to 800 nm. Pink = $IbacF_{20}$, blue = rhodamine 6G, yellow = $BacF_{20}$.

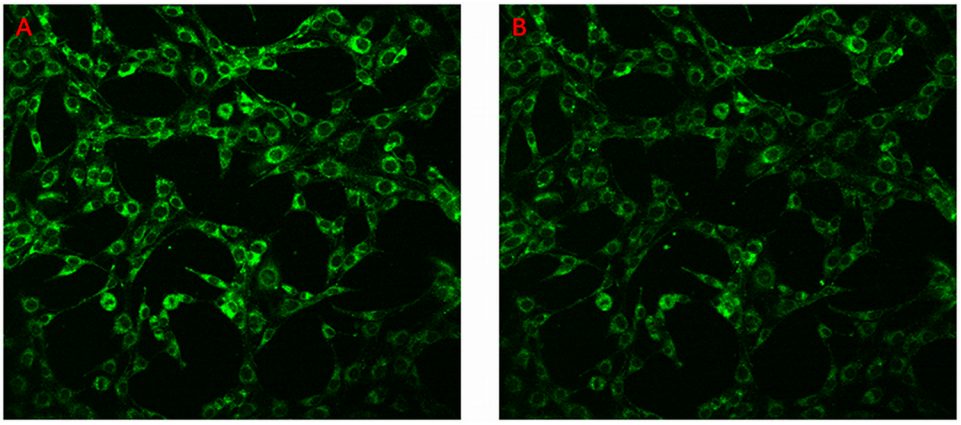

Figure 7.

K:Molv 3T3 NIH cells were incubated with IbacF_{20} for 24 hours and rinsed three times with PBS buffer, the 2-photon microscopy was done repeatedly to examine the photo stability of the compounds under these conditions. Excitation was at 860 nm, and detection between 500 nm and 670 nm. The 2-photon microscopic image after one scan (A), and the same sample after 25 scans (B). The images are as collected.

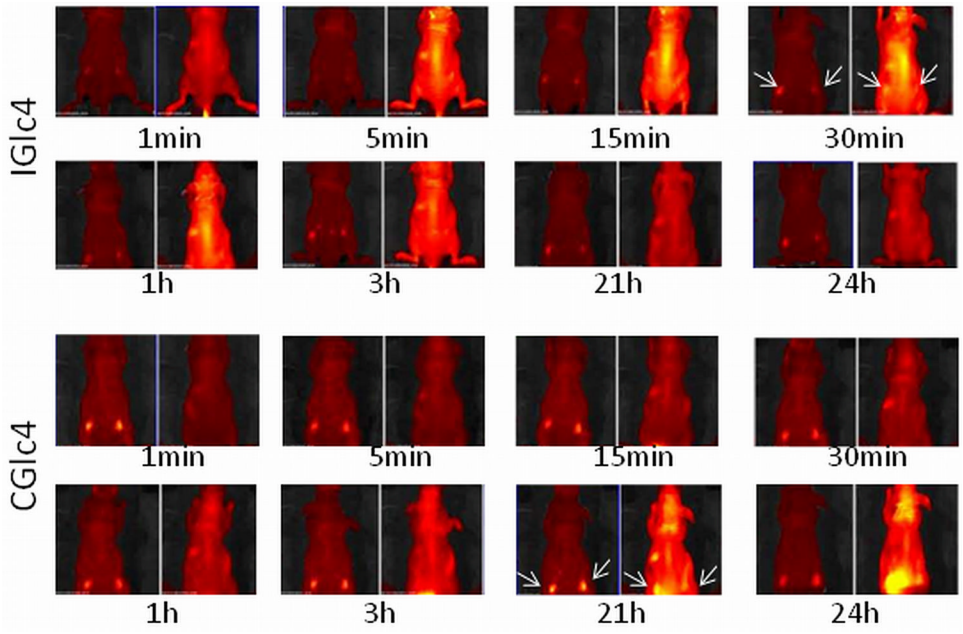

Figure 8.

$IGlc_4$ and $CGlc_4$ up-take, distribution, clearance. Four-week-old, male Balb/c athymic nude mice (Nu/Nu) were obtained from Harlan Sprague Dawley, Inc. (Indianapolis, IN). Mice were housed in temperature-controlled rooms (74 ± 2°F) with a 12-hour alternating light-dark cycle. Approximately 3×10^6 GFP-JHU-22 cells in log phase were injected subcutaneously into the mice. The up-take experiments were done after seven days after GFP-JHU-22 cell inoculation. The mice received tail-vein injections with a total volume of 100 μLof 5mg/mL$IGlc_4$ or $CGlc_4$.The fluorescence images were taken at the times indicated after injection. Each individual group has two images where the emission due to GFP is on the left of each time interval, and monitored using a 465-520 band pass filter. A 605 -660 nm band pass filter was used to image the tumors with $CGlc_4$ and $IGlc_4$. The arrows indicated the location of tumor xenografts. A Xenogren IVIS instrument (Caliper Life Sciences, Hopkinton, MA) was used to collect these images.

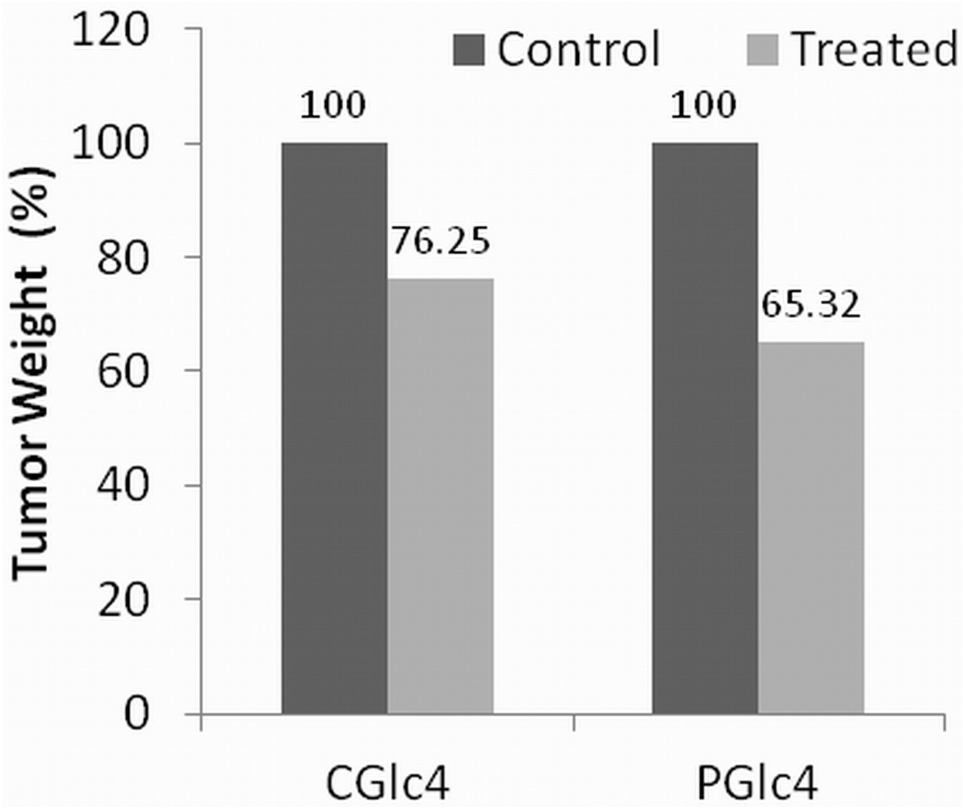

Figure 9.
Decrease in tumor weight after 21 days.

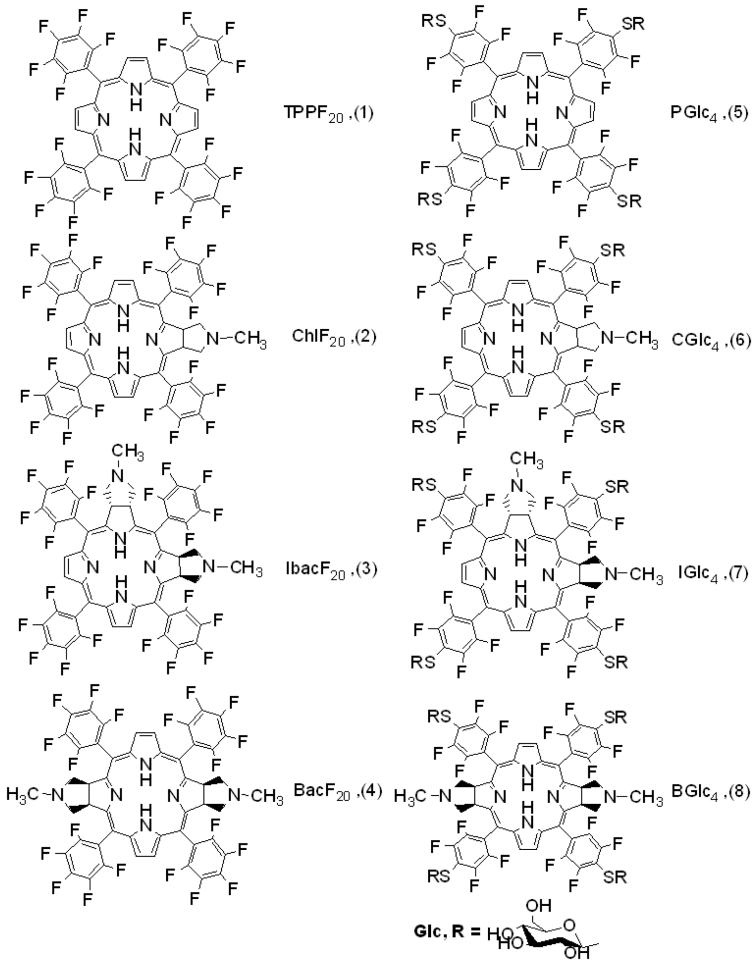

Scheme 1.

Structure of non-glycosylated (**1-4**) and glycosylated (**5-8**) conjugates of porphyrin. The *syn* versus *anti* compounds for the bacteriochlorins and isobacteriochlorins are isolated, but the diastereomers for $CGlc_4$ and two sets of diastereomers for $IGlc_4$ and $BGlc_4$ (see ref. 23) are not separated for these studies.

Table 1

Absorption and emission spectral data of non-glycosylated F_{20} porphyrinoids conjugates.

Comp.	Solvent	UV-visible	Emission
$ChlF_{20}$	ethanol	399, 502, 528, 597, 651	654, 708
	ethylacetate	398, 501, 527, 597, 649	655, 709
$IbacF_{20}$	ethanol	381, 504, 541, 583, 635	592, 645, 707
	ethylacetate	380, 503, 541, 581, 647	594, 645, 711
$BacF_{20}$	ethanol	348, 374, 503, 729	647, 723
	ethylacetate	347, 373, 502, 729	651, 735

Table 2

Photophysical data for compounds **1-8**.

Compound	Solvent	Φ_f	τ_f ns (χ^2)	k_f $(ns)^{-1}$	$(k_f)^{-1}$ ns	k_{nr} $(ns)^{-1}$	$(k_{nr})^{-1}$ ns
$TPPF_{20}$(1)	EA		10.08 (1.21)				
	EtOH		11.14 (1.04)				
$ChlF_{20}$(2)	EA	0.34	7.06 (1.21)	0.048	20.8	0.094	10.6
	EtOH	0.48	7.48 (1.37)	0.064	15.6	0.070	14.3
$IbacF_{20}$(3)	EA	0.60	5.38 (1.25)	0.112	8.9	0.074	13.5
	EtOH	0.72	3.52 (1.19)	0.205	4.9	0.079	12.7
$BacF_{20}$(4)	EA	0.062	6.80 (1.41)	0.009	111.1	0.138	7.3
	EtOH	0.07	6.88 (1.30)	0.010	100.0	0.135	7.4
$PGlc_4$(5)	EA	0.052	9.88 (1.05)	0.0053	188.7	0.096	10.4
	EtOH	0.05	10.84 (1.24)	0.0046	217.4	0.088	11.4
	PBS	0.03	10.66 (1.28)	0.0028	357.1	0.091	11.0
$CGlc_4$(6)	EA	0.39	6.91 (1.42)	0.056	17.9	0.089	11.2
	EtOH	0.43	7.21 (1.34)	0.060	16.7	0.079	12.7
	PBS	0.17	6.84 (1.24)	0.025	40.0	0.121	8.3
$IGlc_4$(7)	EA	0.60	5.93 (1.27)	0.101	9.9	0.068	14.7
	EtOH	0.70	4.29 (1.46)	0.163	6.1	0.070	14.3
	PBS	0.36	2.98 (1.47)	0.121	8.3	0.215	4.7
$BGlc_4$(8)	EA	0.055	7.01 (1.32)	0.0078	128.2	0.135	7.4
	EtOH	0.047	6.96 (1.39)	0.0067	149.3	0.137	7.3
	PBS	0.03	5.44 (1.33)	0.0055	181.8	0.178	5.6

The quantum yield of conjugates **2-4** were calculated in two different solvents, ethanol (EtOH) and ethylacetate.(EA), while phosphate buffered saline (PBS) was also used for **6-8**. The molecules were excited at 509 nm in each case where the O.D = 0.02. TPP was used as reference, Φ_f for TPP in toluene = 0.11. The lifetime of these compounds were measured under argon, by purging argon gas through the cuvette for ca.10 min. The errors in the singlet state lifetime were ± 200 ps, which is the lower limit of time measurement of our instrument.

Table 3

Singlet oxygen quantum yield ($^1O_2\Phi_\Delta$)

compound	$^1O_2\Phi_\Delta$)
$PGlc_4$	0.85
$CGlc_4$	0.32
$BGlc_4$	0.28
$IGlc_4$	0.59

All the compounds were excited at 532 nm in methanol-d_1 solvent; data taken from ref. 23.

Table 4

Two photon cross section values of $IbacF_{20}$

Wavelength (nm)	Cross section (GM)
760	1.7
780	7.5
800	3.2
820	3.1
840	3.2
860	24.5
880	6.1